https://doi.org/10.18321/ectj1499

Effect of Hydration on the Intermolecular Interaction of Various Quaternary Ammonium Based Head Groups with Hydroxide Ion of Anion Exchange Membrane Studied at the Molecular Level

M. Karibayev[1], D. Bekeshov[1], B. Myrzakhmetov[2], S. Kalybekkyzy[2], Y. Wang[1,3], Zh. Bakenov[1,2], A. Mentbayeva[1,2]*

[1]Department of Chemical and Materials Engineering, School of Engineering and Digital Sciences, Nazarbayev University, Kabanbay Batyr ave. 53, Astana, Kazakhstan
[2]Laboratory of Advanced Materials and Systems for Energy Storage, Center for Energy and Advanced Materials Science, National Laboratory Astana, Nazarbayev University, Kabanbay Batyr ave. 53, Astana, Kazakhstan
[3]Laboratory of Computational Materials Science for Energy Applications, Center for Energy and Advanced Materials Science, National Laboratory Astana, Nazarbayev University, Kabanbay Batyr ave. 53, Astana, Kazakhstan

Article info

Received:
20 December 2022

Received in revised form:
17 February 2023

Accepted:
12 April 2023

Keywords:
Ion binding
Hydroxide ion
Quaternary ammonium head group
Hydration level
Anion exchange membranes
Molecular dynamic simulation

Abstract

Currently, the main limitation of Anion Exchange Membrane Fuel Cells is related to their low chemical stability under alkaline conditions due to the degradation of quaternary ammonium-based head groups, which lowers the transportation of hydroxide ions as well. The knowledge of the intermolecular interaction of various quaternary ammonium head groups with hydroxide ions is the key to improving hydroxide ion's diffusivity and chemical stability of various quaternary ammonium-based head groups. Consequently, the intermolecular interaction of hydroxide ions with different quaternary ammonium head groups of anion exchange membranes is investigated at the different hydration levels via classical all-atom Molecular Dynamics and molecular well-tempered MetaDynamics simulation methods in this work. Several quaternary ammonium head groups (a) pyridinium, (b) 1,4-diazabicyclo [2.2.2] octane, (c) benzyltrimethylammonium, (d) n-methyl piperidinium, (e) guanidium, and (f) trimethylhexylammonium were investigated in detail. Classical all-atom molecular dynamic simulations illustrate that the results of radial distribution function between the nitrogen atoms of six different quaternary ammonium head groups and hydroxide ion are as follows: (a) > (c) ≥ (f) > (d) > (e) > (b). In addition, from the diffusion coefficient values it was found that the mobility of hydroxide ion by quaternary ammonium head group (f) was lower than (c) at the different hydration levels.

1. Introduction

Currently, two different hypotheses are being developed in the field of chemistry and biophysics to study the relationship between ions and ligands, such as i) 'ligand field strength' and ii) 'equal affinity' [1, 2]. Earlier studies of the interaction of monovalent with anionic binding sites of glass electrodes in an aqueous solution supported the idea that selective ionic bonds depend mainly on the chemistry of the ligand, which correlated with 'ligand field strength' [3]. According to the 'ligand field strength' hypothesis, binding free energies for alkaline metal ions with ligands should follow the ordered sequence from smaller to larger ion size as

*Corresponding author.
E-mail address: Almagul.mentbayeva@nu.edu.kz

follow: $Li^+ < Na^+ < K^+ < Rb^+ < Cs^+$ [2, 4]. In contrast, the 'equal affinity' hypothesis supports that the binding preference of ion should follow by the cation hydration free energy sequence: $Na^+ < K^+ < Rb^+ < Li^+ < Cs^+$ [5, 6]. Furthermore, the hard and soft acid and base (HSAB) principle was developed to select the ligand for metal ions. According to the HSAB principle, hard acids strongly interact with hard bases and soft acids with soft bases, respectively [7]. The binding of ions to ligands is a fundamental phenomenon in chemistry and biology, having many applications in many systems. However, a significant amount of research has to be carried out on ligand-ion binding phenomena for advanced energy materials such as Anion Exchange Membrane Fuel Cells (AEMFCs). This study will focus on studying the patterns of ligand binding to ionic systems, particularly the binding of quaternary ammonium (QA) to hydroxide (OH^-) ions based on the structure of head groups in AEMFCs.

Hydrogen is produced mainly from methane and is considered an environmentally friendly and easily scalable fuel. The resulting hydrogen fuel and oxygen from the air undergo electrochemical reactions by converting chemical energy into electrical energy in fuel cells [8]. In this regard, AEMFCs attract the attention of scientists due to their low cost, stability, and durability of the material, both cathode kinetics and ohmic polarization. Consequently, scientists are trying to achieve large-scale commercialization of those cells. Anion Exchange Membrane (AEM) is a critical component in such sustainable fuel cell (FC) devices that separates fuel and conducts ions OH^- [9].

AEMFC is a polymer matrix that contains positively charged QA head groups covalently bound to the polymeric backbone [10]. Mainly, these QA head groups determine conducting capacity of the AEMFCs for OH^- ions [11]. According to the available data, there is a significant problem that needs to be solved for large-scale commercialization of AEMFC: The barrier in cell performance stability limits the transportation of OH^- ion due to the chemical degradation reactions of the various QA head groups based polymeric matrix via Hofmann elimination, Nucleophilic Substitution (SN2), and Ylide formation. However, the degradation mechanisms of various QA head groups and OH^- ion transportation mechanisms in high pH are not well understood from insights down to the molecular scale at the different hydration levels (HLs).

Computational modeling and simulations have become critically important tools to explore the chemical degradation and transportation of OH^- ion via positively charged QA head groups of the polymeric backbone of AEM. Particularly, Molecular Dynamics (MD) simulations and Density Functional Theory (DFT) calculations are widely implemented to investigate the nanophase segregation morphology, the diffusivity of OH^- ions in polymeric matrixes of AEM, degradation mechanisms of QA groups of AEM, the effect of HL on the stability of QA head groups and diffusivity of OH^- ion in AEM in the presence of implicit or explicit water [12–27]. In this paper, related computational studies were reviewed at the different multi-length and multi-time-scale [28].

DFT was used to study the interaction and degradation of QA head groups with OH^- ions, as well as to compare theoretical and experimental results obtained from the study of ionic conductivity and chemical stability. The DFT results for the binding energy suggested the following order of the binding strength of OH^- ion with six various QA head groups: (a) > (c) > (f) > (d) > (e) > (b). This suggests that (b) has the highest transport of OH^- ions through the head groups of QA AEM [29]. Considering the Nucleophilic Substitution degradation reactions for QA head groups (c) and (f), the chemical stability of QA (f) was higher than QA (c) [29]. However, molecular Well-Tempered MetaDynamics (WTMD) simulations were not commonly implemented to calculate the binding free energies landscape (FEL) for the association of OH^- ion with the QA head groups of AEM, which is related to chemical stability and transportation phenomena. WTMD simulation is a powerful computational technique to estimate the binding FEL for the association/dissociation of OH^- ion with the QA head group of AEM. The binding FEL calculations mainly provide an efficient route to estimate the dynamic and kinetic characteristics of chemical and biological processes, including ionic conductance or permeability coefficients and association constants that determine the chemical stability and reactivity of designed systems [30]. However, computationally studies of the shielding effect of water solvating the OH^- ions on its nucleophilicity in the presence of QA head groups in combination with experimental properties such as chemical stability and transportation of OH^- ions in AEMFCs are scarce.

In this study, classical all-atom MD simulations, and molecular WTMD simulations were performed to understand the shielding effect of water solvating the OH^- ions in different QA-based head groups. The intermolecular interaction of OH^- ions with the various QA-based head groups of AEM at the different HLs was investigated. Six typical and commonly used QA head groups were selected as theoretical models for classical all-atom MD and molecular WTMD simulations. In the following paragraphs, classical all-atom MD simulations, molecular WTMD simulation methodology, radial distribution function (RDF), coordination number, interaction energy, number of hydrogen bonds, mean squared displacement (MSD), diffusion coefficient, water channel, and binding FEL for OH^- ion with QA-based head groups of AEM, at the different HLs were described.

2. Model and Method

2.1. System of interest

The six different QA head groups of AEM were selected as a computational model for our classical all-atom MD and molecular WTMD simulations, as depicted in Fig. 1. Initially, one molecule of the QA head group from Figure1with one OH^- ion and three water molecules were selected (same as our previous work [29]) for classical all-atom MD and molecular WTMD.

The new systems were created, which contain one/five molecules of QA head group (namely (c) and (f)), one/five OH^- ion, and 3/9/15/500 water molecules were also simulated to explore the effect of HLs and solvation on OH^- ion transportation and chemical stability of AEM via classical all-atom MD, and molecular WTMD.

2.2. Conventional all-atom MD

Initially, the optimized coordinates and force field parameters (partial charges, bonds, angles, dihedrals) for QA head groups (Fig. 1) were generated using the automatic topology building tool Swiss Param (Molecular modeling group, Swiss Institute of Bioinformatics, Lausanne, Switzerland) from optimized ATB database structures [31]. At the same time, Lennard-Jones (LJ) parameters were obtained from the CHARMM36 force field [32]. Each designed system for classical all-atom MD with molecular WTMD simulations includes a single representative segment of the distinctive QA head group with OH^- ion in the presence of explicit TIP3P [33] (3/9/15/500) water molecules. The potential energy of the systems in the CHARMM36 force field includes both bonded/non-bonded contributions [32]. Initial simulation boxes were created with a 500 kJ/mol/nm maximum force limit on each atom using the steepest descent method, to optimize the starting configuration at 1 bar and temperature of 298 K for 0.1 ns, thus energy was minimized. Equilibration of the systems was conducted under NPT and followed by NVT ensembles at 1 bar and 298 K for 1 ns of each. After the system reached equilibrium, production runs for classical all-atom MD simulations were performed for 10 ns with 298 K and 1 bar and with NVT ensemble at a constant volume (Table S1). The LINCS constraint algorithm was implemented for all bonds during the simulation. Therefore, a 0.5 nm cut-off was used for LJ and coulombic short-range interactions. Meanwhile, long-range interactions were computed by Particle Mesh Ewald summation. In addition, a Nose-Hoover thermostat and Berendsen pressure coupling were implemented to maintain temperature

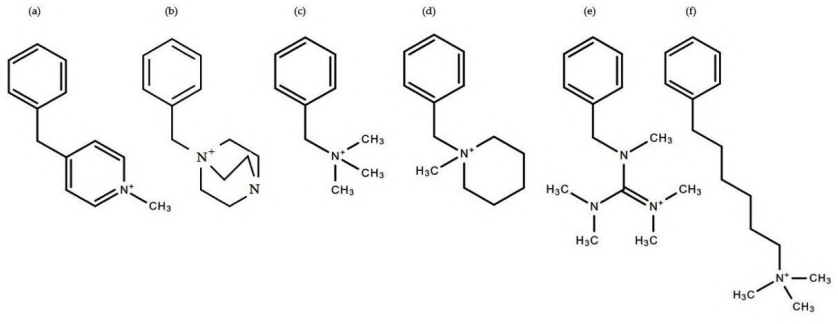

Fig. 1. Structure of representative segments containing different QA head groups. Six different QA head groups are (a) pyridinium, (b) DABCO, (c) BTMA, (d) n-methyl piperi- dinium, (e) guanidium, and (f) TMHA [29].

[34] and system pressure [35], respectively. Note that periodic boundary conditions were introduced in all directions.

The molecular interaction of OH^- ion with six different QA head groups of AEM in the presence of explicit water molecules was studied by classical all-atom MD simulations as can be seen in Table S1. The collective motion of solvent plays a vital role in the transportation of OH^- ions in AEMs which is one of the important aspects of this study. Introducing it could improve the ionic transport channel connectivity and create the QA head groups more flowing and enhance the transportation of OH^- ions. However, there is a lack of profound investigations of the intermolecular interactions between QA head groups of ion transport channels and water molecules. For this reason, classical all-atom MD simulations were applied for studying the nature of OH^- and QA head group interactions by adding explicit water molecules.

Finally, RDF, coordination number, interaction energy, number of hydrogen bonds, MSD, the diffusion coefficient of OH^- ion, and water channel for molecular interaction OH^- ion with six different QA head groups of AEM in the presence of explicit water molecules were analyzed.

2.3. Molecular Well-tempered MetaDynamics

OH^- ions bound with the QA-based head group at the different HL were noted during all-atom MD simulations, which needs to be overcome to estimate the free energy landscape. It was achieved successfully by molecular WTMD simulations, which will be discussed in subsection 3.4. Mainly, the association/dissociation of OH^- ion and QA-based head groups at the different HLs were considered. The important aspects of the OH^- ion QA-based head group is related to the collective motion of water at the different HLs, which plays an important role in the transportation of OH^- ion and chemical stability of various QA head groups of AEM. Due to that reason, molecular WTMD simulations systems for investigating the nature of OH^- and QA-based head group interactions via adding explicit water molecules at the different HLs were applied. Molecular WTMD simulations were performed to obtain free energy landscape (FEL) for our designed systems. In this regard, the FELs were calculated as the distance between the OH^- ion and the QA head group. For our investigated QA (c), the Gaussian hills with a height of 5 kJ/mol and a width of 0.25 Å are deposited every 100 ps [36, 37]. Meanwhile, for our investigated QA (f), the Gaussian hills with a height of 0.4 kJ/mol and a width of 0.35 Å are deposited every 100 ps [37]. Therefore, a careful selection of bias factors is highly important for molecular WTMD. The term "bias factor" relates to the ratio between the temperature of collective variables and the system temperature. That means the bias factor needs to be carefully chosen to cross relevant free energy barriers in the time scale of simulation for various systems. According to the available literature, a bias factor of 25 for QA (c) and 15 for QA (f) based head group segment yielded good results to overcome larger transition barriers for those similar compounds [36]. The molecular WTMD simulation results are analyzed to find the free energy landscape (FEL) of the studied systems, which is crucial to identifying the binding position and local minima. The FELs as a function of the distance between the oxygen atom of the OH^- ion and the nitrogen/carbon atom of the QA-based head group were obtained and discussed. Classical all-atom MD and WTMD simulations were performed in GROMACS software with the PLUMED plugin [38, 39, 40, 41]. In addition, Visualization Molecular Dynamics (VMD) was used to visualize the simulated boxes [42]. In MD simulation, the choice of force-field parameters is essential for our designed system. As a result, the density of the simulation box is approximately 1 g/cm^3 at 298.15 K, 1 bar, which means a good agreement between experimental and computed data and justifies the selection of the force field.

3. Results and discussion

The RDF, coordination number, interaction energies, number of hydrogen bonds, diffusion constants, water channels, and FELs between the nitrogen/carbon atom of QA and the oxygen atom of OH^- ion are analyzed and discussed in subsections 3.1-3.4, respectively.

3.1. Molecular structural properties

3.1.1. Correlation between N atom of QA and OH^- ion

In this study, the RDFs and g(r) profiles (Fig. 2A) were determined for the nitrogen atoms of

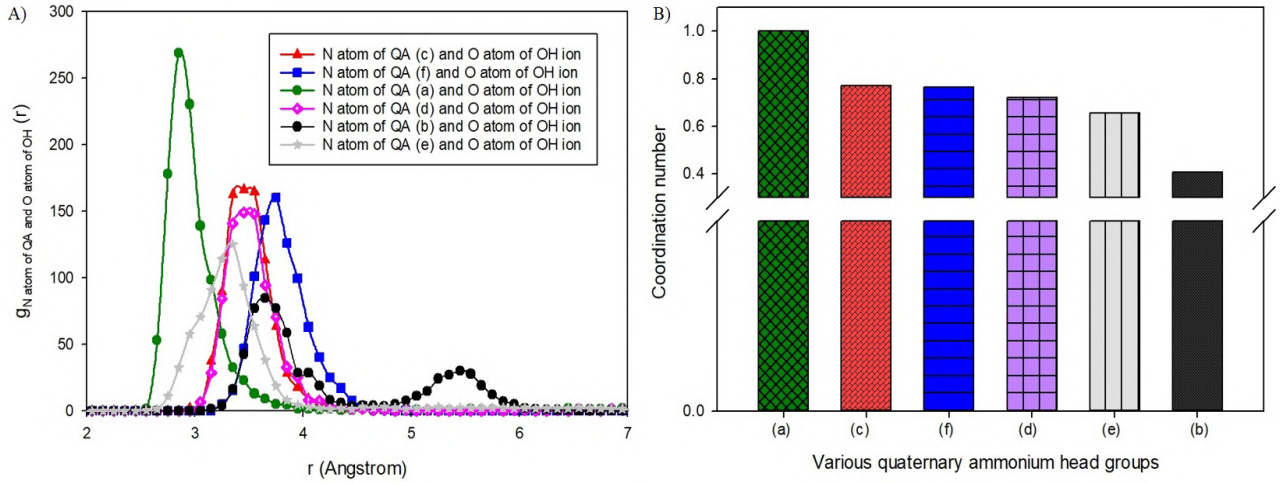

Fig. 2. A) RDFs for nitrogen atom of six various QA head groups with OH^- ion, and then B) the coordination number of six various QA head groups with OH^- ion were illustrated.

the QA head groups with the oxygen atom of OH^- ions. The working process of AEM at HL of 3 is evaluated by RDF results from MD simulations, where the RDFs were depicted as a function of the distance between the oxygen atom of OH^- ions and nitrogen atoms of the six different QA head groups. It was found that the highest electrostatic interaction accounts for the QA head group (a), which holds OH^- ions around it with a peak value of 230.39 at 2.95 Å. The next highest peak value corresponds to the molecular interaction of QA head group (c) with 166.18 at 3.45 Å. The third place in terms of higher peak value was 160.26 at 3.75 Å, which relates for molecular interaction of the QA head group (f) with OH^- ion. Followed by a peak value of 148.98 at 3.45 Å for the QA head group (d). The fifth peak value is around 125.09 at 3.45 Å, which is found for the QA head group (e). The smallest peak corresponds to the QA head group (b) with OH^- ion, and its value of peak was 84.70 at 3.65 Å. In this regard, the order of the molecular interaction strength of OH^- ion with various QA head groups is as follows: (a) > (c) > (f) > (d) > (e) > (b), which could mean (b) have high transportation of OH^- ion via the nitrogen atom of QA head group of AEM. In addition, the coordination numbers were obtained by integrating the RDFs in Fig. 2A up to the first peak, which provides a measure of the number of events for which OH^- coordinates the nitrogen atom of the QA head group sufficiently.

The coordination number was obtained by integrating RDF in spherical coordinates to the first minimum of the RDF value. In this work, the coordination number is defined as the number of OH^- ions that interact with the nitrogen atom of the QA head group. Figure 2B compares the coordination numbers of QA head groups. It was noted that the trend of increasing coordination numbers as follows: (a) > (c) ≥ (f) > (d) > (e) > (b). The interaction strength trend above is also consistent with the experimental results obtained by Yang et al. and our DFT work [43, 29].

Figures 3A and 3B illustrate the RDF profiles between the OH^- ion and nitrogen atoms of QA head group (c) and (f) at the different HL values. According to Fig. 3A, the first highest radial distribution peak value is 176.17 at 3.35 Å, which corresponds to the oxygen of the OH^- ion near the nitrogen atom of a single QA head group (c) at the HL of 3. The second highest peak value is 95.26 at 3.55 Å, which corresponds to HL 9. The third highest peak value is 64.82 at 3.55 Å, which is related to the more weakly bound OH^- ion with the head group QA (c) at HL 15. Figure 3A indicates that the RDFs between OH^- ion and QA head group (c) are weakened with increasing the HL. The same trend was observed for the interaction of OH^- ion with QA head group (f) as a result yielded 160.26 at 3.75 Å for HL 3, 63.66 at 4.35 Å for HL 9, 39.33 at 4.56 Å for HL 15. The intermolecular interaction between the OH^- ion and the nitrogen atom of QA head group ((c) and (f)) was not observed during solvation, according to Figs. 3A and 3B. A high HL is physically shielding the OH^- and consequently, hydration limits the approach of the OH^- ion towards the QA head group, which leads to the decrease of the RDF peak. In this regard,

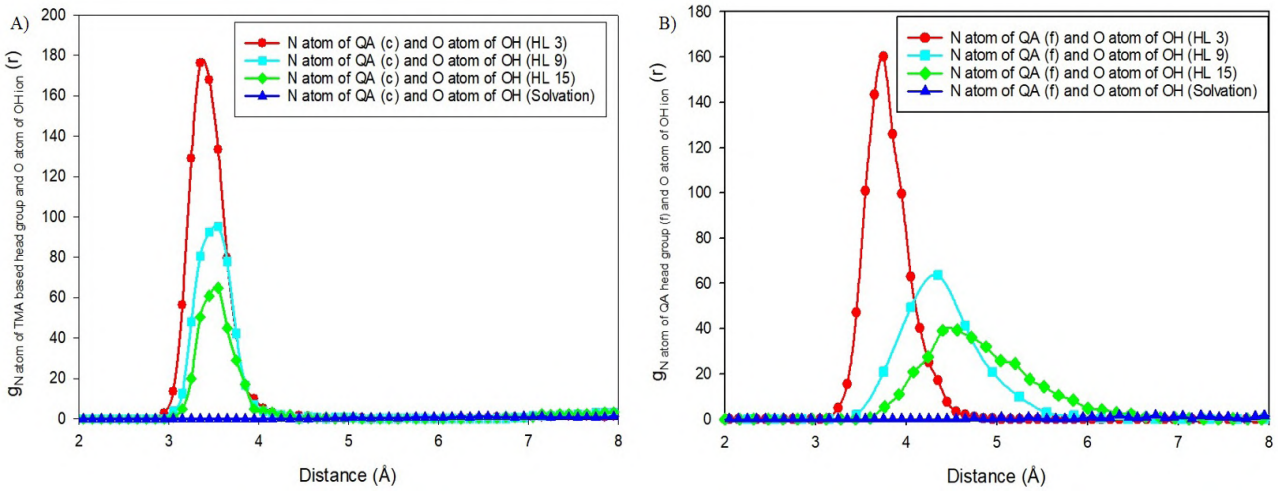

Fig. 3. A) RDFs of the binding OH^- ion with the nitrogen atom of QA head group (c), and B) RDFs of the binding OH^- ion with the nitrogen atom of QA head group (f) in the presence of explicit water at the different HLs.

the correlation of the nitrogen atom of QA based head group site with OH^- ion is decreased as increasing HL, which means lower HL has higher transportation of OH^- ion by the nitrogen atom of QA based head group. In addition, the RDF peak between OH^- ion and QA head group (c) and the RDF peak between OH^- ion and QA head group (f) disappeared at the aqueous media (solvation), which corresponds to the breakdown state of AEM.

3.1.2. Correlation between benzylic C atom of QA and OH^- ion

After that, as can be seen in Fig. 4A, the RDFs, g(r) profiles were calculated for the benzylic carbon atom of the QA head group and the oxygen atom of OH^- ion. Benzylic carbon was selected since it is the site of nucleophilic substitution attack with the lowest activation energy barrier, according to Dekel et al. [44, 45]. Consequently, the highest electrostatic interaction is found for the QA head group (a), as a peak value was 127.84 at 2.90 Å. Recently, resonance stabilized QA head group structure (a) has gained great attention in AEMFC design. QA head group (a) is accepted to have reduced susceptibility toward OH^- attacks because of its delocalized cation structure. However, our results indicate that (a) is the least stable QA head group in the presence of OH^- ion compared to other types of QA head groups. The subsequent highest values of peaks were assigned for molecular interactions of QA head groups (c) and (b)

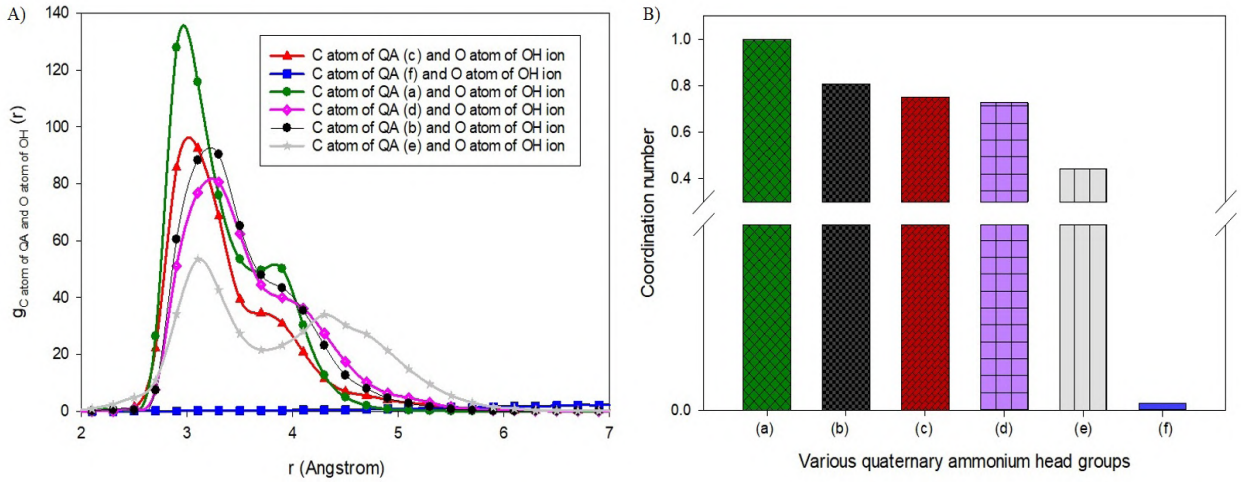

Fig. 4. A) RDFs for benzylic carbon atoms of six various QA head groups with OH^- ion. B) Comparison for a coordination number of degradation of six various QA head groups with OH^- ion.

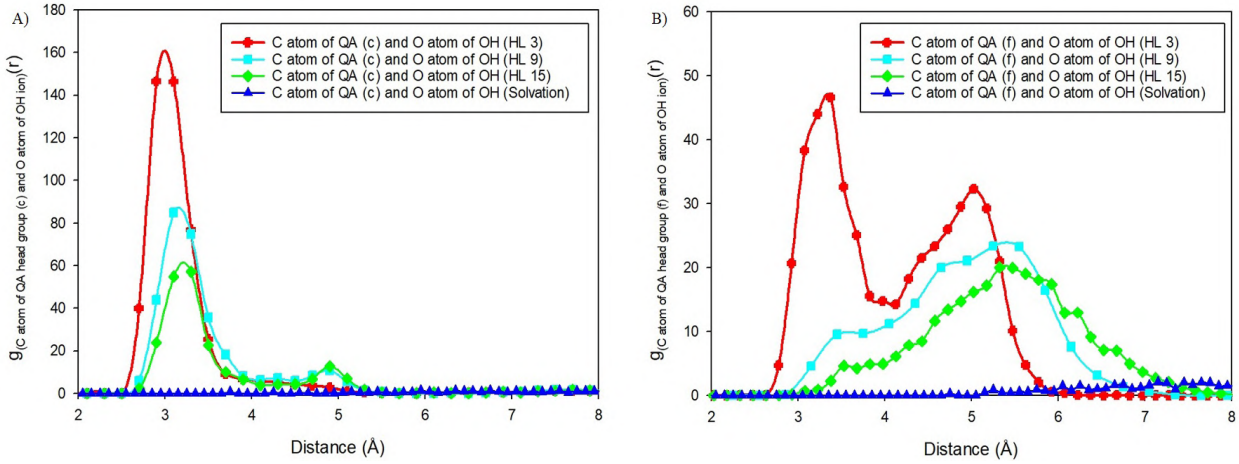

Fig. 5. A) the RDFs of the binding OH^- ion with the carbon atom of QA head group (c), and B) the RDFs of the binding OH^- ion with the carbon atom of QA head group (f) in the presence of explicit water at the different HLs.

with 92.44 at 3.10 Å and 90.34 at 3.30 Å, respectively. Among six model compounds of the QA head groups, two QA head groups ((a), (b)) were found to have lower or similar stability as compared to QA head group (c), while three QA head groups ((d), (e), (f)) illustrated better stability than QA head group (c). The fourth priority in terms of higher peak value was 80.56 at 3.30 Å, which was assigned for molecular interaction of the QA head group (d) with OH^- ion. The fifth peak value is around 53.36 at 3.10 Å, which is found for the QA head group (e). Lastly, the disappearance of the peak at around 3.00 Å supports the observed chemical stability of the QA head group (f). In this regard, the results indicate the trend of increasing stability as follows: (a) < (b) < (c) < d) < (e) < (f). The chemical stability of the QA head group (f) stands out among all six types of QA head groups.

The coordination numbers were obtained by integrating the RDFs in Fig. 4B up to the 4.00 Å, which measures the number of events for which OH^- coordinates the QA head group sufficiently for the degradation reaction to start. Figure 4B compares the coordination numbers of QA head groups. It was highlighted that the trend of increasing stability is as follows: (a) < (b) < (c) < d) < (e) < (f). The alkaline stability trend above is also consistent with the experimental results obtained by Bae et al. and our DFT work [8, 46, 47, 29].

Figures 5A and 5B illustrate RDFs of the OH^- ion around the vicinity of the QA-based head group molecule in the presence of explicit water molecules at the different HLs. As seen in Fig. 5A, the first highest radial distribution peak value is 146.50 at 2.90 Å, which corresponds to the low energy position of the OH^- ion near the benzylic carbon of a single QA head group (c) for HL 3 in a configuration that is prone to degradation. The second highest peak value is 84.97 at 3.10 Å, which corresponds to HL 9 according to Fig. 5A. The third highest peak value is 57.10 at 3.30 Å, which corresponds to more loosely bound OH^- that momentarily bridges several water molecules at HL 15, according to Fig. 5A. The same trend was observed for the interaction of OH^- ion with the QA head group (f) as a result yielded 46.60 at 2.90 Å for HL 3, 23.37 at 5.25 Å for HL 9, 20.03 at 5.32 Å for HL 15 according to Fig. 5B. The intermolecular interaction between OH^- ion and the nitrogen atom of QA head group ((c) and (f)) was not observed during solvation, according to Figs. 5A and 5B. The addition of water hydrates the OH^-, creating a steric shell around the OH^- ion, and as a consequence, RDF peaks tend to move to lower RDF peak values.

Hydration limits the approach of the OH^- ion towards the carbon atom of the QA head group, supporting the observed QA head group stability trend from Figs. 4A and 4B. The alkaline stability trend of radial distribution peaks is also consistent with the experimental and computational results obtained by Dekel et al. [45].

3.2. Bonding properties

3.2.1. Interaction energies between QA head group and OH^- ion

As shown in Table 1, the interaction energies between OH^- ion and QA head group (c) were

-3.330, -0.390, and 0.210 kJ/mol for HL 3, 9, and 15, respectively. In addition, the interaction energies between OH^- ion and QA head group (f) were -2.811, -0.206, and 0.207 kJ/mol for HL 3, 9, and 15, respectively. Consequently, the increase of HLs leads to a decrease in the interaction strength between OH^- ion and QA-based head group. It could be observed that the degradation rate and transportation of OH^- ion took a negative correlation to the interaction between the OH^- ion and the QA-based head group.

The interaction energies between the OH^- ion and QA head group (c) and (f) have been found to be different for HL 3, 9, and 15, with negative values indicating attractive interactions and positive values indicating repulsive interactions. It is interesting to note that the interaction energies decrease as the number of HLs increases, indicating that the strength of interaction between the OH^- ion and the QA-based head group decreases with the increase in HLs.

Table 1
The interaction energies of the binding OH^- ion with QA based head group of AEM in the presence of explicit water at the different HLs.

Binding of OH^- ion with QA head groups	3	9	15
OH^- ion with QA (c) (kJ/mol)	-3.330	-0.390	0.210
OH^- ion with QA (f) (kJ/mol)	2.811	-0.206	0.207

This finding has implications for understanding the behavior of molecules in solution, particularly for understanding the interactions between molecules and their environment. The QA head group is an important functional group in AEMs, and understanding its transportation ability of OH^- ions is critical in AEMFCs.

3.2.2. Hydrogen bonding's between water molecules

The highly hydrated AEM has a relatively high developed hydrogen bonding network [48]. In this regard, the numbers of H-bonding between water molecules at different HLs were calculated, as shown in Table 2.

The results for QA head group (c) revealed 0 hydrogen bonds between water molecules at HL 3; however, the number of hydrogen bonds between water molecules increased from 2 for HL 9 to 8 for HL 15, suggesting the development of hydrogen bonding networks between water molecules. The results for QA head group (f) revealed 0 hydrogen bonds between water molecules at HL 3; however, the number of hydrogen bonds between water molecules increased from 2 for HL 9 to 6 for HL 15, suggesting the development of hydrogen bonding networks between water molecules. Therefore, OH^- transport through the highly hydrated AEM can be determined by the H-bonding internal structure of the formed water channels.

The results presented in the statement suggest that the presence of QA head group (c) and QA head group (f) in the AEM leads to the development of hydrogen bonding networks between water molecules. Specifically, the number of hydrogen bonds between water molecules increases as the HL of the membrane increases, which is indicative of the formation of hydrogen bonding networks.

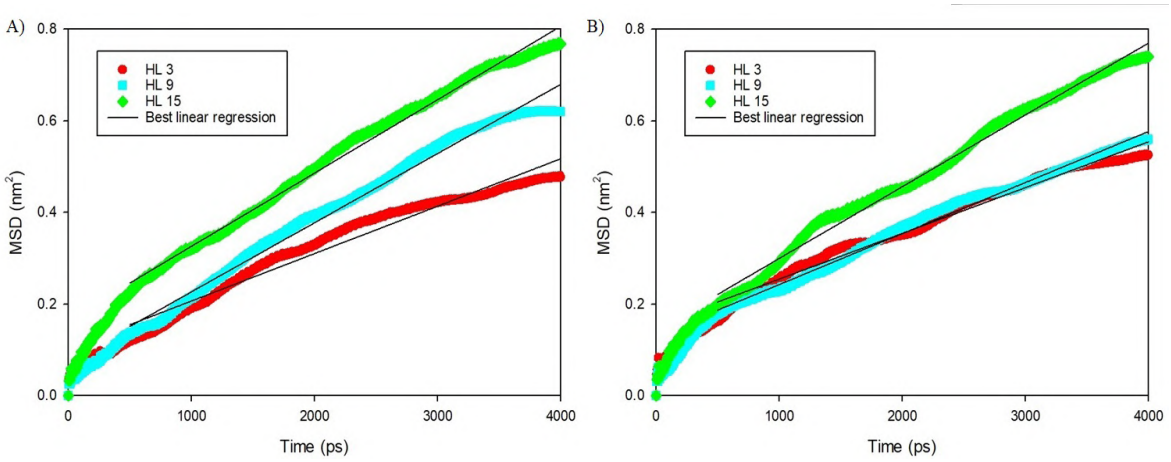

Fig. 6. MSD plot and the trend line at the different HLs for OH^- ions in the presence of A) QA (c), and B) QA (f) head group of AEM.

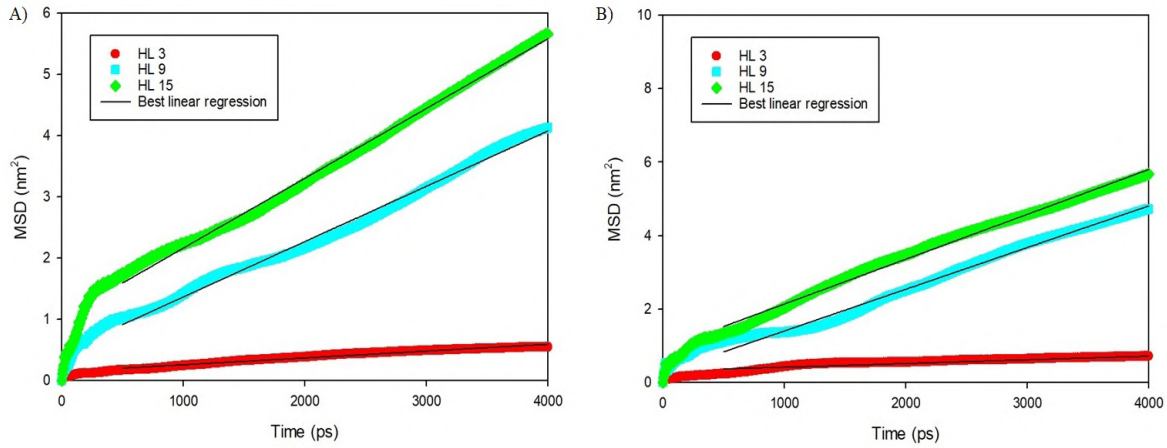

Fig. 7. MSD plot and the trend line at the different HLs for H_2O in the presence of A) QA (c), and B) QA (f) head group of AEM.

Table 2
The number of hydrogen bonds between water molecules of AEM at the different HLs.

Number of H-bonds	3	9	15
Number of H-bonds between H_2O molecules for QA head group (c)	0	2	8
Number of H-bonds between H_2O molecules for QA head group (f)	0	2	6

The absence of hydrogen bonds between water molecules at HL 3 for both QA head group (c) and QA head group (f) suggests that there is insufficient water content in the AEM to facilitate the formation of hydrogen bonding networks. However, as the HL increases, there is a corresponding increase in the bulk water content, which leads to the formation of hydrogen bonding networks.

The formation of hydrogen bonding networks between water molecules is significant because it influences the physical properties of the AEM, including its mechanical strength, swelling behavior, and transport properties. The formation of hydrogen bonding networks can also affect the selectivity of the AEM towards different types of ions and molecules.

The results presented in the statement suggest that the development of hydrogen bonding networks between water molecules is more pronounced for QA head group (c) compared to QA head group (f). This difference in the degree of hydrogen bonding network formation may be due to differences in the chemical structure of the two QA head groups. However, further studies are needed to fully understand the mechanisms underlying the observed differences in hydrogen bonding network formation.

3.3. Mobility of OH^- ion

3.3.1. MSD for OH^- ions, H_2O, and QA at the different HLs

Figures 6–7 show the MSD for OH^- ions, H_2O, and QA at the different HLs, respectively. Further, the diffusion coefficients were calculated from the slope of the MSD curve of OH^- ions, H_2O, and QA at the different HLs. The results of obtained diffusion coefficients were illustrated in Table 3.

Table 3
The diffusion coefficients of AEM components at the different HLs.

Diffusion coefficient, 10^{-5} cm^2/s, (Standard error, 10^{-13}) for	HL		
	3	9	15
OH^- ion in the presence of QA head group (c)	0.017 (0.0024)	0.025 (0.0018)	0.027 (0.0024)
H_2O molecules in the presence of QA head group (c)	0.018 (0.0023)	0.019 (0.009)	0.19 (0.013)
OH^- ion in the presence of QA head group (f)	0.016 (0.0022)	0.018 (0.0019)	0.026 (0.0021)
H_2O molecules in the presence of QA head group (f)	0.018 (0.006)	0.189 (0.012)	0.203 (0.013)

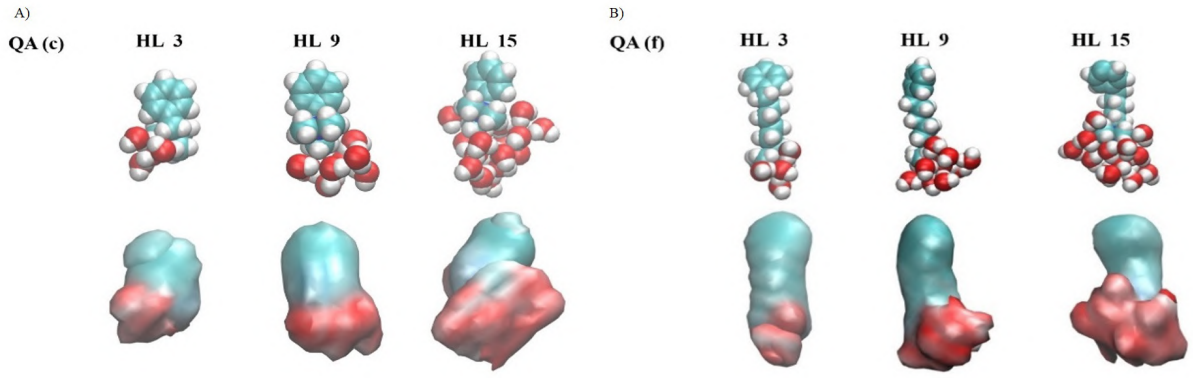

Fig. 8. Snapshot of water channels around A) QA (c) and B) QA (f) at the different HLs.

3.3.2. Diffusion coefficients for OH^- ions, H_2O at the different HLs

As Table 3 indicates, the mobility of OH^- ion, and H_2O molecules increased from HL 3 to HL 15. The diffusion coefficient of OH^- ion, and H_2O molecules increased from 0.017×10^{-5} to 0.027×10^{-5} cm^2/s, and 0.018×10^{-5} to 0.190×10^{-5} cm^2/s, respectively, in the presence of QA head group (c) as an increase of HLs. These findings could mean that the Grotthuss mechanism was the most dominant diffusion mechanism of OH^- ion as HL increases because the Grotthuss mechanism occurs in the bulk of H_2O molecules at a higher HL. As a result, the AEM's ionic conductivity will reach its highest value.

Regarding the TMHA-based head group of AEM, the mobility's of OH^- ion, and H_2O molecules increased from HL 3 to HL 15. The diffusion coefficient of OH^- ion, and H_2O molecules increased from 0.016×10^{-5} to 0.026×10^{-5} cm^2/s, and 0.018×10^{-5} to 0.203×10^{-5} cm^2/s, respectively, in the presence of QA head group (f) as an increase of HLs. These results could reveal that the Grotthuss mechanism was again the most important diffusion mechanism of OH^- ion at a higher HL. At the same time, the working principle of AEMFCs results in gradients in the cell that could lead to low-hydration conditions (HL<5) within the cell.

The higher the water content a cell contained, the monotonically increased mobility of the OH^- ion obtained for QA (c) and QA (f). It could be observed that the mobility of OH^- ions took a positive correlation to the HL and a negative correlation with the interaction between the OH^- ion and the nitrogen atom QA (c)/(f) based head group.

Based on the diffusion coefficients, ionic conductivity (σ) can be calculated using the Nernst-Einstein equation:

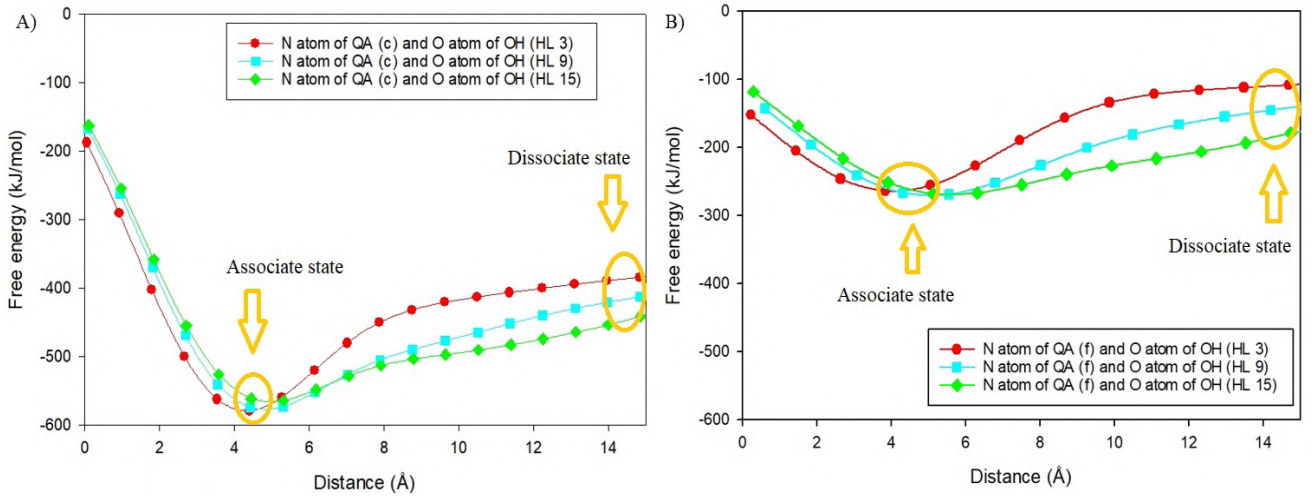

Fig. 9. FEL for binding of OH^- ion with QA based head group at the different HLs as a function of the distance between the oxygen atom of OH^- ion and the nitrogen atom of A) QA (c), and B) QA (f) based head group.

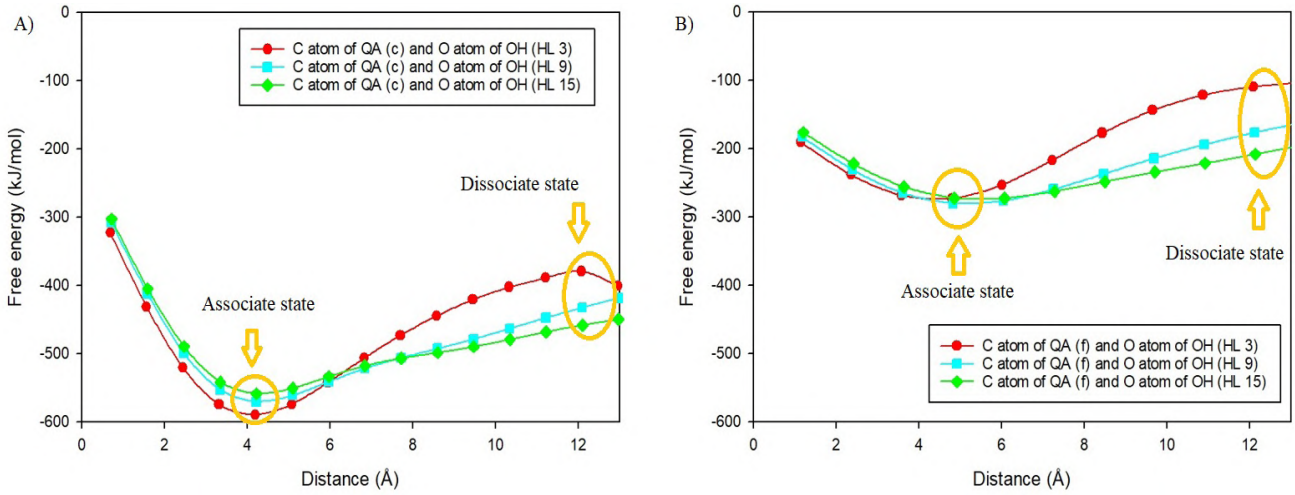

Fig. 10. FEL for binding of OH^- ion with A) QA based head group (c), and B) QA based head group (f) at the different HLs as a function of the distance between the oxygen atom of OH^- ion and the benzylic carbon atom of QA based head group.

$$\sigma = (DNZ^2e^2)/(kBT)$$

where, N is the number density of OH^- ion, Z is the carrier charge, e is the elementary charge, kB is the Boltzmann constant, and T is the absolute temperature. In addition, Zhang et al. stated that the big difference between computationally and experimentally obtained ionic conductivity values [49].

A typical snapshot of an AEM is presented in Figs. 8 A and 8B. The formation of inter-connecting water channels increases by increasing HLs, which is observed and in line with hydrogen bonding analysis.

3.4. Free energy landscapes

The thermodynamic association of OH^- ion with the QA-based head group (c)/(f) segment of AEM at the different HL values was estimated from Figs. 9A and 9B.

It was noted that the relative free energy difference between the associated and the dissociated states of OH^- ion with the nitrogen atom of QA based head group decreases at higher HL values. The association state is a minimum attribute to contact ion pairs, which correspond to the mono-dentate coordination mode of OH^- ion to the QA-based head group of AEM. While the dissociation state is related to the solvent-shared ion pair state, where the ions share appropriately oriented water molecules, each of which forms a hydrogen bond with the OH^- ion and QA-based head group of AEM.

3.4.1. Thermodynamic association between N atom of QA and OH^- ion

According to Fig. 9A, the relative free energy of the difference between the associated and the dissociated states of OH^- ion to QA-based head group is -195.62 kJ/mol, -161.85 kJ/mol, and -123.20 kJ/mol for HL of 3, 9 and 15, respectively.

The similar trend of FELs for the binding mode of OH^- ion to QA-based head group (f) was noted according to Fig. 9B, as the relative free energy differences were -155.65 kJ/mol for HL of 3, -102.46 kJ/mol for HL of 9, and -88.86 kJ/mol for HL of 15. The association and dissociation of the OH^- ions towards the QA head group is limited at higher HL values, via shielding the OH^- ion and leading to the decrease of the binding FEL peak, supporting the observed nitrogen atom of QA head group transportation of OH^- ion trend from classical all-atom MD simulations.

This trend can be explained by the fact that as the HL increases, the distance between the OH^- ion and the QA-based head group also increases. This leads to a decrease in the strength of the electrostatic interactions between the negatively charged OH^- ion and the positively charged QA-based head group. As a result, the relative free energy difference between the associated and dissociated states becomes less negative, indicating a decrease in the binding affinity.

These results have important implications for the design and optimization of AEM-based technologies. In particular, they suggest that the perfor-

mance of AEMs can be optimized by adjusting the HL of the membrane to achieve the desired level of binding affinity. For example, if a high binding affinity is desired, then a lower HL may be preferred in order to maximize the strength of the electrostatic interactions between the OH^- ion and the QA-based head group.

3.4.2. Thermodynamic association between benzylic C atom of QA and OH^- ion

From Fig. 10 the thermodynamic association and dissociation for the oxygen atom of OH^- ion with the benzylic carbon atom of the QA-based head group segment of AEM at the different HLs were estimated. A relative free energy difference of -210.46 kJ/mol corresponds to the HL of 3, -151.63 kJ/mol to 9, and about -108.74 kJ/mol to HL of 15, according to Fig. 10A.

The binding of OH^- ion with the QA-based head group is stronger at lower HLs. A similar trend of FELs for the binding mode of OH^- ion to QA-based head group (f) was observed according to Fig. 10B, as the relative free energy differences were -163.66 kJ/mol for HL of 3, -103.63 kJ/mol for HL of 9, and -78.56 kJ/mol for HL of 15. Hydration limits the pairing of the OH^- ion towards the benzylic carbon atom of QA head group via shielding the OH^- ion, leading to the decrease of the binding FEL peak, supporting the observed stability trend of QA head group from classical all-atom MD simulations.

The observed trend in the FELs can be explained by the electrostatic interactions between the OH-ion and the QA-based head group. At lower HLs, the electrostatic interactions between the negatively charged OH^- ion and the positively charged QA-based head group are stronger due to the shorter distance between them. As the HL increases, the distance between the OH^- ion and the QA-based head group also increases, leading to a decrease in the strength of the electrostatic interactions and consequently the binding affinity.

4. Conclusion

The findings from the all-atom MD simulations with explicit water molecules at different HLs shed light on the intermolecular interaction of OH^- ion with QA-based head groups of AEM. The negative correlation observed between the interaction of OH^- ions with carbon/nitrogen atoms of QA-based head groups and the degradation and transportation of OH^- ions can provide useful insights for the development of more effective AEMs.

Furthermore, the observation that higher water content in the cell leads to increased mobility of OH^- ion obtained for QA (c) and QA (f) highlights the importance of considering water content in the design and optimization of AEMs.

The use of molecular WTMD and classical all-atom molecular dynamics simulations has enabled the scientific community to obtain a more accurate and detailed understanding of the association and dissociation process between QA-based head group of AEM and OH^- ions. The resulting free energy landscape reveals that the relative free energy difference for association and dissociation of OH^- ion with QA-based head group is stronger at lower HLs. These findings provide valuable insights into the fundamental mechanisms underlying this process, which can aid in the development of more effective AEM-based technologies in various fields, including water treatment, energy production, and more. The successful implementation of these simulation techniques highlights the importance of interdisciplinary collaboration and the utilization of advanced computational methods in advancing scientific knowledge.

Overall, these findings demonstrate the potential of computational simulations to provide valuable insights into the behavior and properties of AEMs, which can inform the development of more efficient and sustainable energy technologies.

Acknowledgments

This work was supported by the research grant AP09057868 “High performance polymer-based anion exchange membranes for alkaline fuel cells” projects from MES RK, and 080420FD1906 “Development of composite anion exchange membranes with improved chemical and mechanical stability” from Nazarbayev University.

The authors are also grateful to Nazarbayev University Research Computing for providing computational resources for this work.

Supplementary material

Supplementary material associated with this article can be found, in the online version, at DOI: https://doi.org/10.18321/ectj1499.

References

[1]. Y. Marcus, *J. Chem. Soc., Faraday Trans.* 87 (1991)2995–2999.DOI: 10.1039/FT9918702995

[2]. K.B. Rembert, J. Paterova, J. Heyda, et al., *J. Am. Chem. Soc.* 134 (2012) 10039–10046. DOI: 10.1021/ja301297g

[3]. G. Eisenman, *Biophys. J.* 2 (1962) 259. DOI: 10.1016/s0006-3495(62)86959-8

[4]. M.J. Stevens, S.L. Rempe, *J. Phys. Chem. B.* 120 (2016) 12519–12530. DOI: 10.1021/acs.jpcb.6b10641

[5]. P. Lo Nostro, B.W. Ninham, *Chem. Rev.* 112 (2012) 2286–2322. DOI: 10.1021/cr200271j

[6]. K.D. Collins, *Biophys. J.* 72 (1997) 65–76. DOI: 10.1016/S00063495(97)78647-8

[7]. R.D. Hancock, A.E. Martell, *Chem. Rev.* 89 (1989) 1875–1914. DOI: 10.1021/cr00098a011

[8]. S. Noh, J.Y. Jeon, S. Adhikari, et al., *Acc. Chem. Res.* 52 (2019) 2745–2755. DOI: 10.1021/acs.accounts.9b00355

[9]. V. Vijayakumar, S.Y. Nam, *Ind. Eng. Chem. Res.* 70 (2019) 70–86. DOI: 10.1016/j.jiec.2018.10.026

[10]. B. Bauer, H. Strathmann, F. Effenberger, *Desalination* 79 (1990) 125–144. DOI: 10.1016/0011-9164(90)85002-R

[11]. T. Sata, *J. Membr. Sci.* 167 (2000) 1–31. DOI: 10.1016/S0376-7388(99)00277-X

[12]. S. Chen, H. Wang, J. Zhang, et al., *J. Membr. Sci.* 605 (2020) 118105. DOI: 10.1016/j.memsci.2020.118105

[13]. M.-T. Lee, *J. Phys. Chem. C* 124 (2020) 4470–4482. DOI: 10.1021/acs.jpcc.9b11566

[14]. J. Lu, A. Barnett, V. Molinero, *J. Phys. Chem. C* 123 (2019) 8717–8726. DOI: 10.1021/acs.jpcc.9b01165

[15]. M.-T. Lee, *J. Phys. Chem. C* 123 (2019) 10802–10815. DOI: 10.1021/acs.jpcc.9b01815

[16]. J. Lu, L.C. Jacobson, Y.A. Perez Sirkin, V. Molinero, *J. Chem. Theory Comput.* 13 (2017) 245–264. DOI: 10.1021/acs.jctc.6b00874

[17]. X. Luo, S.J. Paddison, *Solid State Ion.* 339 (2019) 115012. DOI: 10.1016/j.ssi.2019.115012

[18]. Z. Zhu, X. Luo, S.J. Paddison, *Solid State Ion.* 340 (2019) 115011. DOI: 10.1016/j.ssi.2019.115011

[19]. D.J. Kim, C.H. Park, S.Y. Nam, *Int. J. Hydrog. Energy* 41 (2016) 7641–7648. DOI: 10.1016/j.ijhydene.2015.12.220

[20]. H. Takaba, T. Hisabe, T. Shimizu, M.K. Alam, *J. Membr. Sci.* 522 (2017) 237–244. DOI: 10.1016/j.memsci.2016.09.019

[21]. R. Tsuchitani, H. Nakanishi, H. Shishitani, et al., *Solid State Ion.* 278 (2015) 5–10. DOI: 10.1016/j.ssi.2015.05.006

[22]. G.-L. Li, G. Yang, J. Cheng, et al., *J. Phys. Org. Chem.* 31 (2018). DOI: 10.1002/poc.3861

[23]. H. Long, K. Kim, B.S. Pivovar, *J. Phys. Chem. C.* 116 (2012) 9419–9426. DOI: 10.1021/jp3014964

[24]. T. Xiang, H. Si, *Comput. Theor. Chem.* 1065 (2015) 12–17. DOI: 10.1016/j.comptc.2015.04.022

[25]. S. Chempath, J.M. Boncella, L.R. Pratt, et al., *J. Phys. Chemis. C* 114 (2010) 11977–11983. DOI: 10.1021/jp9122198

[26]. S. Castaneda, R. Ribadeneira, *J. Phys. Chem. C* 119 (2015) 28235–28246. DOI: 10.1021/acs.jpcc.5b07166

[27]. S. Chempath, B.R. Einsla, L.R. Pratt, et al., *J. Phys. Chem. C* 112 (2008) 3179–3182. DOI: 10.1021/jp7115577

[28]. M. Karibayev, S. Kalybekkyzy, Y. Wang, A. Mentbayeva, *Molecules* 27 (2022) 3574. DOI: 10.3390/ molecules27113574

[29]. M. Karibayev, B. Myrzakhmetov, S. Kalybekkyzy, et al., *Molecules* 27 (2022) 2686. DOI: 10.3390/molecules27092686

[30]. A. Pohorille, C. Jarzynski, C. Chipot, *J. Phys. Chem. B* 114 (2010) 10235–10253. DOI: 10.1021/jp102971x

[31]. K.B. Koziara, M. Stroet, A.K. Malde, A.E. Mark, *J. Comput. Aided Mol. Des.* 28 (2014) 221–233. DOI: 10.1007/s10822-014-9713-7

[32]. P. Bjelkmar, P. Larsson, M.A. Cuendet, et al., *J. Chem. Theory Comput.* 6 (2010) 459–466. DOI: 10.1021/ct900549r

[33]. W.L. Jorgensen, J. Chandrasekhar, J.D. Madura, et al., *J. Chem. Phys.* 79 (1983) 926–935. DOI: 10.1063/1.445869

[34]. P. Podio-Guidugli, *J. Elast.* 100 (2010) 145–153. DOI: 10.1007/s10659-010-9250-0

[35]. H.J.C. Berendsen, *Comput. Simul. Mat. Sci.* (1991) 139–155. DOI: 10.1007/978-94-011-3546-7_7

[36]. F. Sicard, T. Bui, D. Monteiro, et al., *Langmuir* 34 (2018) 9701–9710. DOI: 10.1021/acs.langmuir.8b01366

[37]. J. Hinks, Y. Wang, W.H. Poh, et al., *Langmuir* 30 (2014) 2429–2440. DOI: 10.1021/ la403409t

[38]. M. Bonomi, G. Bussi, C. Camilloni, et al., *Nat. Methods.* 16 (2019) 670–673. DOI: 10.1038/s41592-019-0506-8

[39]. G.A. Tribello, M. Bonomi, D. Branduardi, et al., *Comput. Phys. Commun.* 185 (2014) 604–613. DOI: 10.1016/j.cpc.2013.09.018

[40]. M. Bonomi, D. Branduardi, G. Bussi, et al., *Comput. Phys. Commun.* 180 (2009) 1961–1972. DOI: 10.1016/j.cpc.2009.05.011

[41]. D. Van Der Spoel, E. Lindahl, B. Hess, et al.,

J. Comput. Chem. 26 (2005) 1701–1718. DOI: 10.1002/jcc.20291

[42]. W. Humphrey, A. Dalke, K. Schulten, *J. Mol. Graph.* 14 (1996) 33–38. DOI: 10.1016/0263-7855(96)00018-5

[43]. G. Yang, J. Hao, J. Cheng, N. Zhang, G. He, F. Zhang, C. Hao, *Int. J. Hydrog. Energy* 41 (2016) 6877–6884. DOI: 10.1016/j.ijhydene.2016.03.067

[44]. D.R. Dekel, M. Amar, S. Willdorf, et al., *Chem. Mater*. 29 (2017) 4425–4431. DOI: 10.1021/acs.chemmater. 7b00958

[45]. D.R. Dekel, S. Willdorf, U. Ash, et al., *J. Power Sources* 375 (2018) 351–360. DOI: 10.1016/j.jpowsour.2017.08.026

[46]. A.D. Mohanty, S.E. Tignor, M.R. Sturgeon, et al., *J. Electrochem. Soc.* 164 (2017) F1279. DOI: 10.1149/2.0141713jes

[47]. A.D. Mohanty, C. Bae, *J. Mater. Chem. A* 2 (2014) 17314–17320. DOI: 10.1039/C4TA03300K

[48]. K.W. Han, K.H. Ko, K. Abu-Hakmeh, et al., *J. Phys. Chem. C* 118 (2014) 12577–12587. DOI: 10.1021/jp412473j

[49]. N. Zhang, J. Huo, B. Yang, et al., *Chem. Eng. Sci.* 192 (2018) 1167–1176. DOI: 10.1016/j.ces.2018.08.051